Finite-volume effects and dynamical chiral symmetry breaking in QED_3

Tobias Goecke,[1] Christian S. Fischer,[1,2] and Richard Williams[1]
[1]*Institute for Nuclear Physics, Darmstadt University of Technology, Schlossgartenstraße 9, 64289 Darmstadt, Germany*
[2]*GSI Helmholtzzentrum für Schwerionenforschung GmbH, Planckstr. 1, 64291 Darmstadt, Germany*
(Received 14 November 2008; published 11 February 2009)

We investigate the impact of finite-volume effects on the critical number of flavors, N_f^c, for chiral symmetry restoration in QED_3. To this end we solve a set of coupled Dyson-Schwinger equations on a torus. For order parameters such as the anomalous dimension of the fermion wave function or the chiral condensate, we find substantial evidence for a large dependence on the volume. We observe a shift in N_f^c from values in the range of $3.61 \leq N_f^c \leq 3.84$ in the infinite-volume and continuum limit down to values below $N_f \leq 1.5$ at finite volumes in agreement with earlier results of Gusynin and Reenders in a simpler truncation scheme. These findings explain discrepancies in N_f^c between continuum and lattice studies.

DOI: 10.1103/PhysRevB.79.064513 PACS number(s): 11.10.Kk, 11.15.Tk, 12.20.−m

I. INTRODUCTION

Dynamical chiral symmetry breaking in the theory of quantum electrodynamics in (2+1) dimensions (QED_3) (Ref. 1) has been studied quite intensively over the years. The problem is of considerable interest for two reasons. On one hand, QED_3 has enough similarities to quantum chromodynamics (QCD) such that analogies to the more complicated non-Abelian case may be drawn. On the other hand, QED_3 itself is of considerable interest due to possible applications in condensed-matter systems.

In particular, QED_3 with $N_f=2$ flavors of massless fermions has been suggested as an effective low-energy theory of high-T_c cuprate superconductors.[2–4] These possess an unconventional *d*-wave symmetry of the pairing condensate, with nodes at the electronic Fermi surface allowing for a description in terms of massless nodal quasiparticles. The quasiparticles do not couple to an external electromagnetic field and hence represent pure spin degrees of freedom; a spin-charge separation has taken place. The interaction of these spinons with the collective topological excitations of the gap can be described by a U(1) gauge theory. Since furthermore the motion of the quasiparticles is mainly confined to the two-dimensional copper-oxygen planes in these systems, one ends up with quantum electrodynamics in (2+1) dimensions. Depending on whether the system is ordered or disordered it is either in an insulating quantum antiferromagnetic (AF) phase or a pseudogap (PG) phase with remnant properties of the underlying superconductor. In the gauge theory the AF phase corresponds to a phase with broken chiral symmetry and long-range correlations due to massless photons. In the PG phase the fermions are massless and the fermion wave function as well as the photon propagator develop power laws at small momenta with a fractional anomalous dimension.[3,5]

The above considerations explain the interest in determining N_f^c, the critical number of fermion flavors for the chiral phase transition of QED_3. If $N_f^c > 2$ then the effective low-energy theory is chirally broken at zero temperature. For the superconductor this means that the theory displays a phase transition between the superconducting and the antiferromagnetic phase when doping is varied.[2,3] If on the other hand $N_f^c < 2$ the system goes from a superconducting to a pseudogap phase when underdoped.

The value of N_f^c has been investigated in a number of studies from Dyson-Schwinger equations (DSEs) in the continuum[3,5–14] and lattice gauge theory.[15–19] While the former allows for numerical as well as analytical studies in principle there remains the question of the importance of truncation artifacts. For N_f^c a partial answer has been obtained in Ref. 5, where it was found that the details of the fermion-photon vertex only have a minor quantitative impact on N_f^c. In particular for all vertex dressings employed N_f^c stayed well above $N_f=2$.

In all studies of dynamical chiral symmetry breaking in continuum QED_3 a clear separation of scales has been found. The intrinsic scale of the theory is given by the dimensionful coupling constant $\alpha=N_f e^2/8$. Then a second and much lower scale is given by the dynamically generated fermion mass $M(0)$ in the chiral limit. Related to this one has small values for the other order parameter, the chiral condensate. On the lattice with its finite volume this separation of scales is hard to bridge. Consequently, recent studies for two flavors[17] and four flavors[17,18] determined bounds on the chiral condensate, but no definite value for N_f^c could be extracted. A definite signal for chiral symmetry breaking was obtained only for one flavor.[18] A very recent calculation claims that $N_f^c \approx 1.5$ with the caveat of volume and discretization artifacts.[19]

In general, the presence of an infrared (IR) cutoff due to the finite volume reduces the value of the critical number of flavors. This was demonstrated by Gusynin and Reenders[20] in a simple truncation scheme for the DSEs. They considered an approximation to the DSE for the fermion self-energy which neglects corrections to the fermion wave function and the fermion-photon vertex. The photon is then given by its leading behavior in the $1/N_f$ expansion. In this work we elaborate on these findings by considering a more sophisticated truncation scheme which explicitly takes into account nonperturbative effects in all of these quantities. In addition we follow a different strategy to assess the volume effects by evaluating the system on a three-torus. A corresponding technique has been applied in QCD_4 to determine finite-volume effects in the quark and gluon propagators.[21–23]

This work is organized as follows. In Sec. II we recall results for QED_3 in the infinite-volume and continuum limit.

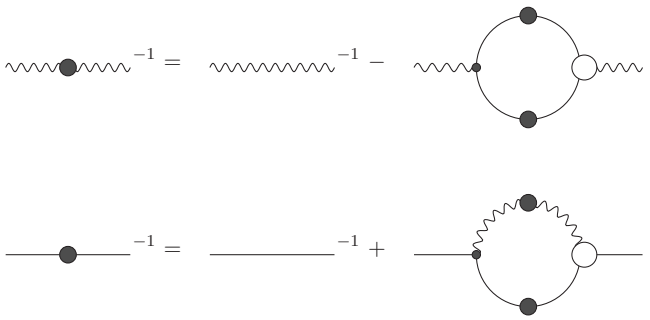

FIG. 1. The Dyson-Schwinger equations of the photon and fermion propagators in diagrammatic notation. Wiggly lines denote photon propagators and straight lines the fermion. A black dot denotes a bare fermion-photon vertex, while the open circle denotes a dressed one.

We present the Dyson-Schwinger equations for the fermion and photon propagators and discuss their asymptotic properties. In Sec. III we recall general conditions for chiral symmetry breaking on a finite volume, formulate the DSEs in a box, and discuss our numerical methods to solve these. In Sec. IV we present our numerical results for the propagators at finite volume and the critical number of flavors N_f^c as a function of the box size. In Sec. V we conclude.

II. QED$_3$ IN THE INFINITE-VOLUME AND CONTINUUM LIMIT

A. Dyson–Schwinger equations in QED$_3$

We consider QED$_3$ with a four-component spinor representation for the Dirac algebra and N_f fermions. This allows a definition of chiral symmetry similar to the cases of QED$_4$ and QCD$_4$. With massless fermions, the Lagrangian has a U($2N_f$) "chiral" symmetry, which is broken to SU(N_f) $\times$SU(N_f)$\times$U(1)$\times$U(1) if the fermions become massive. The order parameter for this symmetry breaking is the chiral condensate which can be determined, e.g., via the fermion propagator.

The Dyson-Schwinger equations for the photon and fermion propagators in Euclidean space are given diagrammatically in Fig. 1. They read explicitly

$$D_{\mu\nu}^{-1}(p) = D_{0,\mu\nu}^{-1}(p) - Z_1 N_f e^2 \int \frac{d^3q}{(2\pi)^3} \mathrm{Tr}[\gamma_\mu S(q) \Gamma_\nu(q,k) S(k)], \tag{1}$$

$$S^{-1}(p) = S_0^{-1}(p) + Z_1 e^2 \int \frac{d^3q}{(2\pi)^3} \gamma_\mu S(q) \Gamma_\nu(q,p) D_{\mu\nu}(k), \tag{2}$$

with the momentum routing $k_\mu = q_\mu - p_\mu$. Here N_f denotes the number of fermion flavors and Z_1 is the renormalization constant of the fermion-photon vertex Γ_ν.

In Landau gauge the general form of the dressed fermion propagator $S(p)$ and the photon propagator $D_{\mu\nu}(p)$ is given by

$$S(p) = \frac{i\not{p} A(p^2) + B(p^2)}{p^2 A^2(p^2) + B^2(p^2)}, \tag{3}$$

$$D_{\mu\nu}(p) = \left(\delta_{\mu\nu} - \frac{p_\mu p_\nu}{p^2}\right) \frac{G(p^2)}{p^2} = \left(\delta_{\mu\nu} - \frac{p_\mu p_\nu}{p^2}\right) \frac{1}{p^2[Z_3 + \Pi(p^2)]}, \tag{4}$$

with the photon dressing function $G(p^2)$, the photon polarization $\Pi(p^2)$, and renormalization function Z_3 and the fermion dressing functions $A(p^2)$ and $B(p^2)$. These can be rearranged into the renormalization-group invariant fermion mass function $M(p^2) = B(p^2)/A(p^2)$ and the fermion wave function $Z_f(p^2) = 1/A(p^2)$. Another renormalization-group invariant is the "running coupling" $e^2 G(p^2)$ built from the renormalization-point-dependent photon dressing function $G(p^2)$ and the renormalized coupling e^2. The bare-renormalized fermion propagator is given by $S_0^{-1}(p) = Z_2(i\not{p} + Z_m m)$, where m is the renormalized current fermion mass, Z_m is the mass-renormalization function, and Z_2 the corresponding one for the fermion wave function. Note that in QED we have the Ward-Takahashi identity $Z_1 = Z_2$.

The gauge dependence of the fermion mass and wave function and, correspondingly, the fermion-photon vertex has been a much debated issue in the past, see, e.g., Refs. 5 and 24–32 and references therein. There in particular the technical question of how to truncate the fermion-photon interaction to obtain a gauge covariant pattern of chiral symmetry breaking and restoration has been discussed. This issue is not quite settled yet; however there are clear indications[5,32,33] that Landau gauge is preferred in the sense that it allows for particularly simple approximation schemes. In all other linear covariant gauges parametrized by the gauge parameter ξ a gauge-dependent scale $\frac{\xi e^2}{8\pi}$ appears which complicates matters considerably. This is why we choose Landau gauge in this work.

A range of *Ansätze* for the fermion-photon vertex have been investigated in Ref. 5. There it has been found that the critical number of flavors N_f^c obtained with the most elaborate construction, obeying the Ward-Takahashi identity, is almost similar to the one of the most simple *Ansatz*, a bare-renormalized vertex,

$$\Gamma_\nu = Z_1 \gamma_\nu. \tag{5}$$

Therefore to keep matters as simple as possible we will only present results for the bare vertex approximation in this work. We did check, however, that more sophisticated *Ansätze* do not alter the main conclusions presented below. In addition, a general analysis of the infrared behavior of QED$_3$ in the framework of functional renormalization-group equations indicates that in Landau gauge bare vertex (5) may even be the best possible choice.[33]

Substituting this vertex into the fermion and photon DSEs, taking appropriate traces and contracting the photon DSE with the projector,

$$\mathcal{P}_{\mu\nu}(p) = \delta_{\mu\nu} - \zeta \frac{p_\mu p_\nu}{p^2}, \tag{6}$$

with $\zeta=1$ we arrive at

$$B(p^2) = Z_2 Z_m m + Z_2^2 e^2 \int \frac{d^3q}{(2\pi)^3} \frac{2B(q^2)}{q^2A^2(q^2)+B^2(q^2)} \frac{G(k^2)}{k^2}, \tag{7}$$

$$A(p^2) = Z_2 + Z_2^2 e^2 \int \frac{d^3q}{(2\pi)^3} \frac{A(q^2)}{q^2A^2(q^2)+B^2(q^2)} \frac{G(k^2)}{k^2} \times \left(-\frac{k^2}{2p^2} + \frac{(p^2-q^2)^2}{2k^2p^2} \right), \tag{8}$$

$$\frac{1}{G(p^2)} = Z_3 + \Pi(p^2) = Z_3 - Z_2^2 e^2 N_f \int \frac{d^3q}{(2\pi)^3} \times \frac{1}{q^2A^2(q^2)+B^2(q^2)} \frac{1}{k^2A^2(k^2)+B^2(k^2)} \tilde{W}_1(p^2,q^2,k^2), \tag{9}$$

where we used $Z_1=Z_2$ and the subtracted kernel,

$$\tilde{W}_1(p^2,q^2,k^2) = W_1(p^2,q^2,k^2) - \frac{2k^2(3-\zeta)}{3p^2}, \tag{10}$$

with

$$W_1(p^2,q^2,k^2) = \frac{\zeta k^4}{p^4} + k^2\left(\frac{1-\zeta}{p^2} - \frac{2\zeta q^2}{p^4} \right) - 1 + \frac{(1-\zeta)q^2}{p^2} + \frac{\zeta q^4}{p^4} \tag{11}$$

in the photon equation. As explained in Appendix A of Ref. 5 the subtraction of the term proportional to $(3-\zeta)$ in Eq. (10) is necessary to avoid spurious linear divergences in the photon-DSE generated by the regularization procedure (a hard cutoff) used in the numerical treatment of the equations. The choice $\zeta=1$, i.e., the transverse projection of the photon equation, is mandatory to avoid the backreaction of spurious longitudinal terms into the right-hand side of the photon equation. Compared to Ref. 5, where $\zeta=3$ has been used, this treatment leads to a quantitatively improved value for the critical number of flavors (see below). Note, however, that the effects of varying ζ are quantitatively small in general; all qualitative conclusions derived in Ref. 5 and also here are independent of the choice of ζ.

B. Asymptotic behavior of the propagators

An often used approximation to determine the asymptotic behavior of the fermion and photon dressing functions has been the $1/N_f$ expansion. This expansion is equivalent to a perturbative expansion for small e^2 while keeping $\alpha = N_f e^2/8$ fixed. As QED_3 is an asymptotically free theory this expansion does provide correct answers in the ultraviolet. For the photon polarization and the vector dressing function of the fermion one finds for N_f massless fermion flavors,[6]

$$\Pi(p^2 \gg \alpha) = \frac{N_f e^2}{8p} = \frac{\alpha}{p}, \tag{12}$$

$$A(p^2 \gg \alpha) = 1. \tag{13}$$

For the mass function of the fermion one can use the operator product expansion to obtain

$$M(p^2 \gg \alpha) = \frac{2+\xi}{4} \frac{\langle \bar{\Psi}\Psi \rangle}{p^2}, \tag{14}$$

with the chiral condensate $\langle \bar{\Psi}\Psi \rangle$. Note that the condensate can also be determined from the trace of the fermion propagator:

$$\langle \bar{\Psi}\Psi \rangle = -4Z_2 \int \frac{d^3q}{(2\pi)^3} \frac{B(q^2)}{q^2A^2(q^2)+B^2(q^2)}. \tag{15}$$

In the infrared-momentum region the $1/N_f$ expansion is clearly not sufficient. Here one has to resort to a self-consistent analysis of the DSEs in terms of asymptotic power laws. This method is well developed in QCD_4 (Refs. 34–37) and has been adapted to QED_3 in Ref. 5. Such an analysis is valid if no scales are present, i.e., in the deep infrared-momentum region $p \ll \alpha$ and only in the absence of fermion masses. The appearance of infrared power laws with potentially fractional anomalous dimensions is thus an indicative and characteristic property of the symmetric phase of QED_3.

For a bare fermion-photon vertex the infrared behavior of the vector fermion dressing function and the photon polarization in the chirally symmetric phase can be written as

$$A(p^2) \sim p^{2\kappa}, \quad \Pi(p^2) \sim p^{-1-4\kappa}. \tag{16}$$

In case of a dressed fermion-photon vertex according to the Ward-Takahashi identity the corresponding power laws are

$$A(p^2) \sim p^{2\kappa}, \quad \Pi(p^2) \sim p^{-1-2\kappa}. \tag{17}$$

These expressions solve the DSEs in the chirally symmetric phase as described in detail in Ref. 5 (see also Ref. 32 for a rederivation from a slightly different perspective).

The value of κ as a function of N_f can then be determined from the DSEs using a procedure given in detail in Ref. 5. The solutions for a bare vertex with and without the subtracted term in Eq. (10) is plotted in Fig. 2. For $N_f > 1.5$ the exact solutions can be represented by the fits

$$\kappa_{\text{bare}}^{\text{sub}} = \frac{0.142}{N_f} + \frac{0.002}{N_f^2} + O\left(\frac{1}{N_f^3}\right), \tag{18}$$

$$\kappa_{\text{bare}} = \frac{0.137}{N_f} + \frac{0.058}{N_f^2} + O\left(\frac{1}{N_f^3}\right). \tag{19}$$

A corresponding fit for the bare vertex and a Ward-Identity improved vertex for $\zeta=3$ is given in Ref. 5. The difference between Eqs. (18) and (19) represents the systematic uncertainty in our numerical calculation due to the cut-off regularization procedure used. For dimensional regularization the subtraction of the term in Eq. (10) is not necessary, and

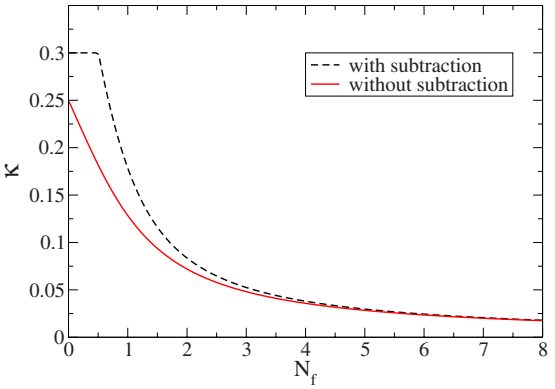

FIG. 2. (Color online) The infrared exponent κ as a function of the number of flavors N_f in the symmetric phase of QED_3.

therefore the unsubtracted result [Eq. (19)] should be viewed as the exact one for the bare vertex truncation scheme. In principle one can reproduce Eq. (19) also in a numerical treatment of the DSEs with a hard cutoff when vertex corrections around the cut-off scale are included (see Ref. 38 for details). However, this procedure is much more involved than the simple subtraction scheme of Eq. (10). Since the difference between Eqs. (18) and (19) is rather small in the interesting region above $N_f=2$ and therefore unimportant for all of the conclusions of the present work, we resort to the simple subtraction scheme [Eq. (10)] and consequently reproduce Eq. (18) in our numerics.

The critical number of flavors N_f^c where chiral symmetry is restored can be determined analytically from the DSE for the scalar fermion dressing function $B(p^2)$. Again we refer the reader for details to Ref. 5 and merely state the result

$$(N_f^c)_{\text{bare}}^{\text{sub}} \approx 3.84, \tag{20}$$

$$(N_f^c)_{\text{bare}} \approx 3.61. \tag{21}$$

The corresponding result from the functional renormalization group[33] is $(N_f^c)_{\text{bare}} \approx 3.6$, in agreement with our result for the unsubtracted equation. Numerical results for Ward-identity improved vertices[5] lead to results in the range of 3.5–4. These numbers can be contrasted with $(N_f^c)_{1/N_f}=32/\pi^2 \approx 3.24$ from the $1/N_f$-expansion.[7] Note that all these results are far above $N_f=2$ relevant for the description of high-T_c cuprate superconductors as discussed in Sec. I.

Finally we wish to emphasize that these power-law solutions can only be obtained when the full structure of the propagator DSEs is taken into account. The authors of Refs. 9 and 10 did not find a solution corresponding to a symmetric phase in their truncation scheme because the feedback from the function A onto the vacuum polarization is not taken into account. This then prohibits the appearance of power laws and therefore does not allow for the appearance of the chirally symmetric phase and should be discarded.[5,32]

III. QED_3 AT FINITE VOLUMES

A. Chiral symmetry breaking in a box

Before we embark on our investigation, let us recall the general finite-volume behavior of the chiral condensate.[39] The fermion propagator in its spectral representation is given by

$$S_A(x,y) = \sum_n \frac{u_n(x)u_n^\dagger(y)}{m - i\lambda}, \tag{22}$$

where $u_n(x)$ and λ_n are the eigenfunctions and eigenvalues of the Euclidean Dirac operator, $\not{D}u_n(x)=\lambda_n u_n(x)$. The gauge field A is treated as an external field. These eigenfunctions occur either as zero modes or in pairs of opposite eigenvalues. Setting $x=y$, integrating over x, and neglecting the zero mode contributions, one obtains

$$\frac{1}{V}\int_V S_A(x,x) = -\frac{2m}{V}\sum_{\lambda_n>0}\frac{1}{m^2+\lambda_n^2}. \tag{23}$$

The chiral condensate can be deduced by averaging the left-hand side of this equation, over all gauge-field configurations, and then taking the infinite-volume limit to give

$$\langle \bar{q}q \rangle = -2m\int_0^\infty d\lambda \frac{\rho(\lambda)}{m^2+\lambda^2}, \tag{24}$$

where $\rho(\lambda)$ is the mean level density of the spectrum, which becomes dense in the infinite-volume limit. In the chiral limit, $m\to 0$, only the infrared part of the spectrum contributes and one finally arrives at the Banks-Casher relation,[40]

$$\langle \bar{q}q \rangle = -\pi\rho(0). \tag{25}$$

If the two limits are interchanged, i.e., if one takes the chiral limit before the infinite-volume limit, one has a discrete sum in Eq. (23) and the infrared part of the spectrum cannot trigger a nonvanishing chiral condensate: chiral symmetry is restored. If, however, at a given volume the explicit fermion mass m is not too small, one can still observe the spontaneous formation of a quark condensate. If the factor $(m^2+\lambda_n^2)^{-1}$ varies only slightly with n, the sum in Eq. (23) can still be replaced by an integral and Eq. (25) remains valid. For this to be a legitimate approximation one needs $m \gg \Delta\lambda \sim 1/V\rho(\lambda) = \pi/(V|\langle \bar{q}q \rangle|)$, at the lower end of the spectrum. Thus one obtains the condition,[39]

$$Vm|\langle \bar{q}q \rangle| \gg \pi. \tag{26}$$

This relation reveals the crux of the matter. In principle, if the volume is large enough, the necessary quark masses are academically small and may even be neglected in the numerical treatment. What counts as *large* in this context, however, depends sensitively on the size of the chiral condensate. In QED_3 the condensate becomes extremely small already well below the critical number of flavors N_f^c of the chiral phase transition.[5] Thus although a formulation on a finite volume may do well for $N_f=1$, all signals of dynamical chiral symmetry breaking will be lost already well below the N_f^c of the theory in the infinite-volume and continuum limit. This behavior will be quantified below.

B. DSEs on a torus

On a compact manifold, the photon and fermion fields have to obey appropriate boundary conditions in the time

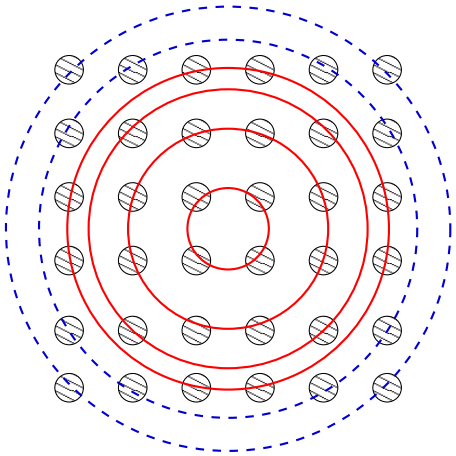

FIG. 3. (Color online) Two-dimensional sketch of the momentum grid dual to the three-torus for a fixed Cartesian momentum cutoff. The hyperspheres depicted by dashed lines are not complete in the sense that additional momentum points on these spheres are generated if the cutoff is increased. The torus equivalent of an O(3)-invariant cutoff used in our calculations sums only over complete hyperspheres, which are indicated by fully drawn circles.

direction. These have to be periodic for the photon fields and antiperiodic for the fermions. For computational reasons it is highly advantageous, although not necessary, to choose the same conditions in the spatial directions. We choose the box to be of equal length in all directions, $L_1=L_2=L_3\equiv L$, and denote the corresponding volume $V=L^3$. Together with the boundary conditions this leads to discretized momenta in momentum space. Thus all momentum integrals appearing in the Dyson-Schwinger equations are replaced by sums over Matsubara modes.

On a torus with antiperiodic boundary conditions for the fermion fields, the momentum integral changes into a sum of Matsubara modes,

$$\int \frac{d^3q}{(2\pi)^3}(\cdots) \to \frac{1}{L^3}\sum_{n_1,n_2,n_3}(\cdots), \tag{27}$$

counting momenta $\mathbf{q_n}=\Sigma_{i=1..3}(2\pi/L)(n_i+1/2)\hat{e}_i$, where $\hat{e}_i$ are the Cartesian unit vectors in Euclidean momentum space. For the photon with periodic boundary conditions the momentum counting goes like $\mathbf{q_n}=\Sigma_{i=1..3}(2\pi/L)(n_i)\hat{e}_i$. For the numerical treatment of the equations it is convenient to rearrange these summations such that they represent a spherical coordinate system,[21] see Fig. 3 for an illustration. We then write

$$\frac{1}{L^3}\sum_{n_1,n_2,n_3}(\cdots) = \frac{1}{L^3}\sum_{j,m}(\cdots), \tag{28}$$

where j counts spheres with $\mathbf{q_n}\mathbf{q_n}=$const and m numbers the grid points on a given sphere. The corresponding momentum vectors are denoted by $\mathbf{q}_{m,j}$ and their absolute values are given by $q_{m,j}=|\mathbf{q}_{m,j}|$. It is then a simple matter to introduce the torus equivalent of an $O(3)$-invariant cutoff by restricting j to an interval $[1, N]$. This procedure is equivalent to "cutting the edges" of our torus as indicated in Fig. 3.

The resulting DSEs are then given by

$$B(p_{i,l}^2) = Z_2 Z_m m + Z_2^2 \frac{e^2}{L^3}\sum_{j,m}^{N} \frac{2B(q_{j,m}^2)}{q_{j,m}^2 A^2(q_{j,m}^2) + B^2(q_{j,m}^2)} \frac{G(k_{i,l,j,m}^2)}{k_{i,l,j,m}^2}, \tag{29}$$

$$A(p_{i,l}^2) = Z_2 + Z_2^2 \frac{e^2}{L^3}\sum_{j,m}^{N} \frac{A(q_{j,m}^2)}{q_{j,m}^2 A^2(q_{j,m}^2) + B^2(q_{j,m}^2)} \frac{G(k_{i,l,j,m}^2)}{k_{i,l,j,m}^2} \times\left(-\frac{k_{i,l,j,m}^2}{2p_{i,l}^2} + \frac{(p_{i,l}^2 - q_{j,m}^2)^2}{2k_{i,l,j,m}^2 p_{i,l}^2}\right), \tag{30}$$

$$\frac{1}{G(p_{i,l}^2)} = Z_3 - Z_2^2 \frac{e^2 N_f}{L^3}\sum_{j,m}^{N} \frac{1}{q_{j,m}^2 A^2(q_{j,m}^2) + B^2(q_{j,m}^2)} \times \frac{1}{k_{i,l,j,m}^2 A^2(k_{i,l,j,m}^2) + B^2(k_{i,l,j,m}^2)} \tilde{W}_1(p_{i,l}^2, q_{j,m}^2, k_{i,l,j,m}^2). \tag{31}$$

Note that the momentum argument k of the photon self-energy in the fermion DSE is the difference $k_{i,l,j,q}=p_{i,l}-q_{j,q}$ of two antiperiodic Matsubara momenta and thus lives on a momentum grid corresponding to periodic boundary conditions, as it should.

The DSEs can be solved numerically employing well-established methods. Our numerical method on the torus is outlined in Ref. 22, the corresponding continuum method as well as details on the renormalization procedure of the DSEs are given in Ref. 5.

Note that the propagators determined from the continuum version of the DSEs, Eqs. (7)–(9) are independent of the regularization procedure. In our numerical calculations in the infinite-volume and continuum limit we use a subtracted version of these equations and an O(3)-invariant UV cutoff which can be sent to infinity at the end of each calculation. These DSEs therefore represent not only the infinite-volume limit but also the continuum limit (in coordinate space) of the representation given by Eqs. (7)–(9) of the DSEs on a torus. We use the phrase infinite-volume and continuum limit to indicate this simultaneous removal of both an ultraviolet and an infrared cutoff.

IV. NUMERICAL RESULTS

A. Finite-size effects: Fixing the UV cutoff

Before we investigate the finite-volume effects of various quantities of interest we have to clarify whether there are sizable effects due to the finite size of the system corresponding to a fixed ultraviolet momentum cutoff. Part of these effects are removed by our choice of cutting the edges of the torus described in Sec. III. The remaining finite-size effects can be evaluated by varying the size of the cutoff. Here, a natural minimal cutoff is given by the intrinsic scale $\alpha=N_f e^2/8$ of QED$_3$. Thus, working in the range $0<N_f\leq 8$, we anticipate that finite-size effects are of minor importance for cutoffs larger than the intrinsic scale, i.e., $\Lambda^2\geq e^4$. Indeed, this is the case as can be seen from the two plots in Fig. 4.

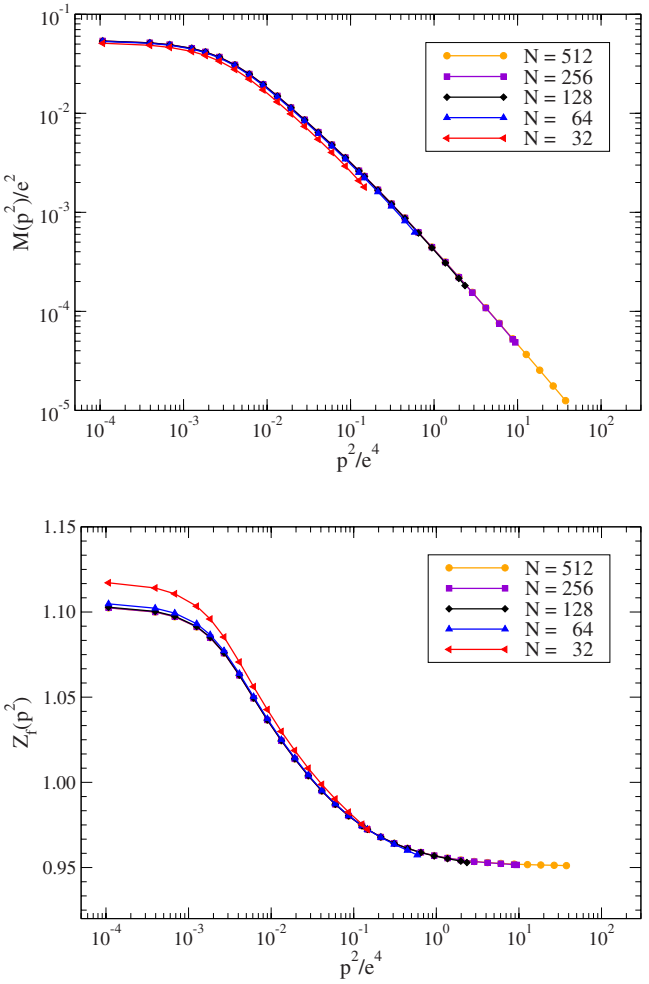

FIG. 4. (Color online) Fermion mass function $M(p^2)$ and wave function $Z_f(p^2)$ as a function of scaled momentum p^2/e^4. The volume of the box corresponding to the smallest available momentum is kept fixed and the ultraviolet cutoff is varied. Here N counts the number of momentum points in one direction of our torus, i.e., $N=100$ means that we employed a torus with 200^3 momentum vectors. This translates into the cutoffs $\Lambda^2_{\mathrm{UV}}=0.15e^4, 0.62e^4, 2.47e^4, 9.86e^4, 39.5e^4$.

Shown are the fermion mass function $M(p^2)$ and wave function $Z_f(p^2)$ as a function of scaled momentum p^2/e^4 for various cutoffs between $\Lambda^2_{\mathrm{UV}}=0.15e^4$ and $\Lambda^2_{\mathrm{UV}}=39.5e^4$. The number of fermion flavors is chosen to be $N_f=1$, similar results are obtained for other choices. The box volume for the fermions is related to the lowest momentum point p^2_{min} by $V=L^3$, with $L=\sqrt{3}\pi/p_{\mathrm{min}}$. Here we use $L=390/e^2$. Note that for the photon the box volume is related to the lowest momentum point by $V=L^3$, with $L=2\pi/p_{\mathrm{min}}$. The same box length then results in a slightly different value for the lowest momentum point in the photon dressing function. We refrain from showing the photon explicitly here since the finite-size effects are similar to the ones for the fermions.

In Fig. 4 the finite-size effects are visible only for the smallest cutoff. There are effects in both the infrared and ultraviolet momentum regions, where a number of momentum points deviate from the results with larger cutoffs. This is true for the renormalization-point-dependent fermion wave function (normalized to match the continuum result) but also for the renormalization-point-independent fermion mass function. The perhaps surprising observation that the variation in an ultraviolet cutoff also affects the infrared behavior of the dressing functions implies a certain entanglement between the infrared and ultraviolet modes of a gauge theory. Similar effects have been found in four-dimensional Yang-Mills theory, see, e.g., Ref. 38 and references therein.

We also need to comment on the fact that we observe dynamical chiral symmetry breaking in our system at all despite in practice working with a vanishing bare quark mass. In the continuum formulation this entails working in the chiral limit. However, due to the formal reasons discussed in Sec. III A this cannot be true on a finite volume since taking the chiral limit before the infinite-volume limit inevitably leads to the loss of dynamical chiral symmetry breaking. However, this is not what we observe here. Indeed, the volumes we use are large enough to allow for extremely small bare fermion masses according to the relation of Eq. (26). In practice, this allows one to neglect the fermion mass entirely in the numerical treatment of the DSEs. However it is important to keep in mind that this means we are working *close* to the chiral limit but not *in* the chiral limit.

We conclude Sec. IV A with the observation that from about $\Lambda^2_{\mathrm{UV}}=e^4$ onwards almost no finite-size effects are present. We therefore consider this value a lower bound for admissible cutoffs on a torus, in agreement with our general considerations concerning the natural scale in QED_3. This finding also agrees with corresponding results on finite-size effects in lattice simulations, see Ref. 19 and references therein. In order to be absolutely sure that cut-off effects do not play any role in what follows we use the somewhat larger cutoff $\Lambda^2_{\mathrm{UV}}=2.35e^4$ from now on.

B. Finite-volume effects: Toward the infinite-volume limit

We are now in a position to study the finite-volume effects occurring for the fermion and photon propagators on a torus. To this end we keep the ultraviolet cutoff of our system fixed and vary the infrared cutoff in the range of $Le^2=200-3000$. We show the resulting behavior of the fermion mass and wave function as well as the photon together with the corresponding continuum results in Fig. 5. Again, we choose $N_f=1$. The variation in the volume clearly results in the loss of a substantial amount of generated fermion mass when the volume gets smaller and smaller. For even smaller volumes than shown in the figure chiral symmetry is restored in agreement with the condition $Vm|\langle\bar{q}q\rangle| \gg \pi$ discussed in Secs. III A and IV A. On the other hand, we observe that extremely large volumes are needed to account for the full effect of dynamical chiral symmetry breaking observed in the infinite-volume and continuum limit. This is in marked contrast with the behavior of the quark sector of QCD_4 (Ref. 41) and can be explained by a closer look at the scales involved. Whereas in QCD_4 the generated quark masses $[M(0)\approx 300-400\ \mathrm{MeV}]$ are of the same order as the intrinsic scale of the system ($\Lambda^{\bar{MS}}_{\mathrm{QCD}}\approx 250\ \mathrm{MeV}$), the situation is clearly different in QED_3. Here our characteristic scale is of the order of $\alpha=e^2/8$, whereas the generated fermion masses

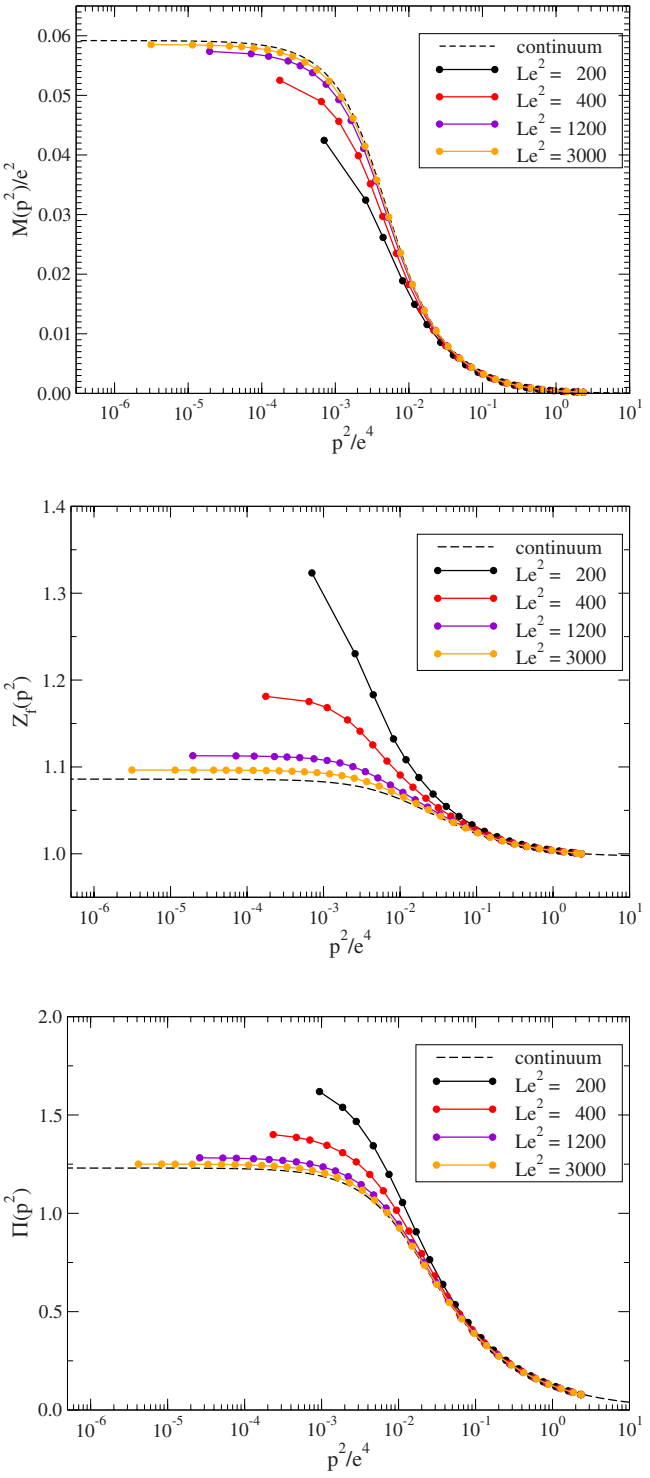

FIG. 5. (Color online) Fermion mass function $M(p^2)$, wave function $Z_f(p^2)$, and photon self-energy $\Pi(p^2)$ as a function of scaled momentum p^2/e^4. The ultraviolet momentum cutoff is kept fixed at $\Lambda_{\mathrm{UV}}^2=2.35e^4$ and the box length is varied from $Le^2=200-3000$.

are of order of $10^{-2}e^2$ as can be seen from the plot. To keep volume effects small, this scale has to be well accommodated by the system on a box, which translates to a lowest momentum to be much smaller than $p^2=10^{-5}e^4$. Indeed, this is what we observe. Choosing the volume large enough that the lowest momentum is well below this scale, we approach the infinite-volume and continuum limit. This is true for all three dressing functions; the fermion mass function $M(p^2)$, the fermion wave function $Z_f(p^2)$, and the photon self-energy $\Pi(p^2)$.

C. Finite-volume effects: $Z_f(N_f)$ and $\kappa(N_f)$

Let us now examine the influence of finite-volume effects on the critical value N_f^c, where the system undergoes a phase transition from the chirally broken into the chirally symmetric phase. This phase transition is marked by the change in the infrared asymptotics of the fermion wave function $Z_f(p^2)$; for $N_f<N_f^c$ this function is a constant in the infrared, whereas for $N_f>N_f^c$ it develops a power law with N_f-dependent exponent κ, see Ref. 5. In a sense, κ can be viewed as an order parameter of this phase transition. (Note, however, that this transition is not a first-order or second-order one but has properties of a conformal phase transition.[42]) We exhibit this behavior of κ by fitting a power law in the infrared to the fermion wave function,

$$Z_f(p^2) = C(p^2)^{-\kappa}, \tag{32}$$

which is related to the fermion vector dressing function by $Z_f=1/A$. Both, the coefficient C and the power κ may depend on N_f.

To visualize this procedure the fermion wave function Z is shown in the upper panel of Fig. 6 for a box with $Le^2 \approx 800$ for different numbers of flavors N_f. One clearly sees the aforementioned behavior: for $N_f \leq 2.0$ the function develops a constant in the infrared region (i.e., $\kappa=0$) whose value is proportional to N_f. The phase transition occurs for this specific volume for $2.0<N_f^c<2.2$. For $N_f \geq 2.2$ one observes a power law of the wave function at small momenta. The coefficient of this power law is still proportional to N_f; however the exponent κ decreases with growing N_f according to Eq. (18). Consequently we observe a decrease in the function $Z_f(p^2)$ with growing N_f in the symmetric phase. As a result one could determine N_f^c as the number of flavors for which Z_f is maximal at a given infrared momentum. This is also the case in the infinite-volume and continuum limit.[5]

As an (equivalent) alternative we determine N_f^c by fitting power law (32) to our numerical results for $Z_f(p^2)$ in the infrared-momentum region. There is a caveat here: similar to four-dimensional Yang-Mills theory one observes that power law (32) can only be seen for momenta $1/L \ll p \ll e^2$. This behavior is generic on a torus.[23] To obtain significant results for our infrared coefficients we therefore have to perform the fit for momentum points significantly larger than the lowest one. In practice we chose momenta from the fourth point onwards.

The resulting dependence of the exponent κ on N_f is plotted in the lower panel of Fig. 6 for several volumes of the box together with the corresponding function in the infinite-volume and continuum limit. At infinite volume the function $\kappa(N_f)$ is zero for $N_f<N_f^c \approx 3.84$ and equal to the analytic result of Eq. (20) in the symmetric phase above N_f^c. For a given finite volume the phase transition is still indicated by a maximum in $\kappa(N_f)$. However, there is an additional region at

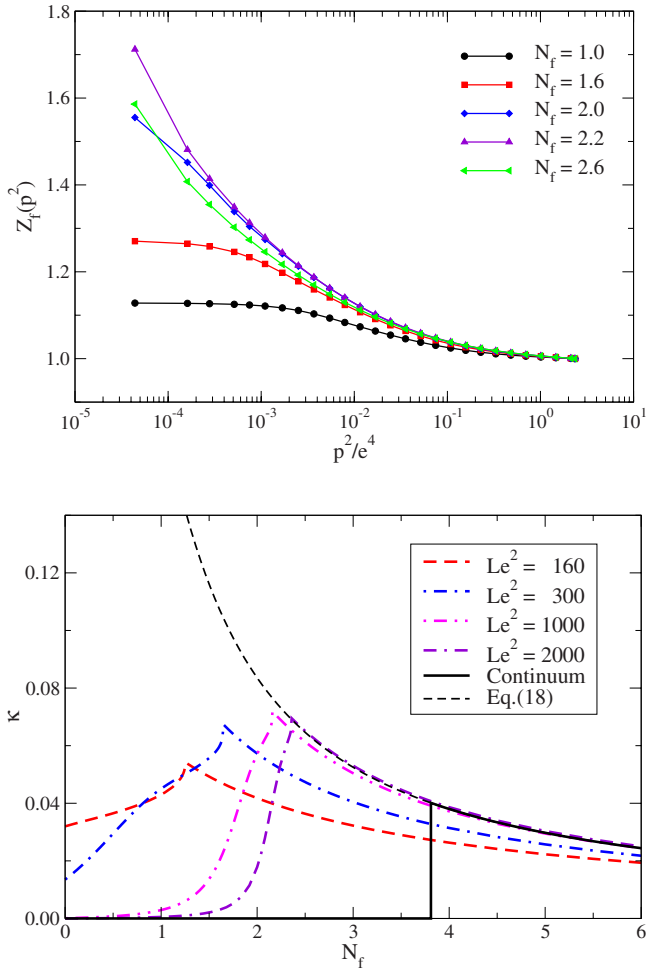

FIG. 6. (Color online) Upper plot: Fermion wave function $Z_f(p^2)$ as a function of scaled momentum p^2/e^4 and the number N_f of fermion flavors. Note that for clarity of the figure from $p^2/e^4 = 10^{-3}$ upwards only results for a selected number of momentum points on the torus are shown. Lower plot: The resulting value of the infrared exponent κ as a function of N_f for different volumes.

$N_f < N_f^c(L)$, where the function rises slowly toward its maximal value. This region is generated by the finite infrared cutoff of the system in a box, which prevents the fermion wave function $Z_f(p^2)$ from bending toward a finite asymptotic value at $p^2=0$. This effect mimics a power law at values of N_f where the system is still in the chirally broken phase. With increasing volume this region gets smaller and smaller until it reaches the sharp rise of the function in the infinite-volume and continuum limit as shown in Fig. 6.

As a result we find a critical number of flavors which depends upon the volume of the torus. The explicit values are shown in Fig. 7 together with corresponding results from Ref. 20. In the following we concentrate on the solutions close to the chiral limit and postpone the discussion of the (orange) curve with large bare fermion mass to Sec. IV C.

For volumes that are not too large, our solutions and the ones reported in Ref. 20 can be well fitted by a form,

$$N_f^c = a - \frac{b}{(Le^2)^{1/3}}. \tag{33}$$

For our results we obtain $a=3.23$ and $b=10.64$, shown as

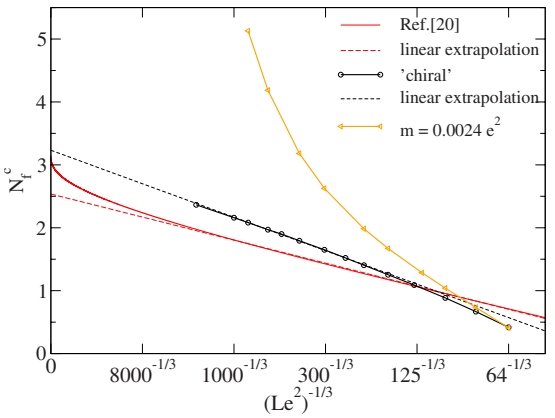

FIG. 7. (Color online) The critical number of flavors N_f^c as a function of inverse box length $1/L^{1/3}$. In the chiral limit we show the results of our calculation (chiral) compared to the corresponding one of Ref. 20 in a simpler truncation scheme. The dashed lines are linear extrapolations to the infinite-volume limit. We also show results for a bare fermion mass $m=0.0024e^2$ comparable to the ones used in lattice calculations.

dashed line in the plot. Interestingly, to high precision the exponent of the box length in this fit is given by $-1/3$ although we do not have a good explanation for exactly this behavior. In terms of $(1/L)^{1/3}$ the fit then suggests a linear extrapolation to the infinite-volume limit. However, it turns out that this linear behavior breaks down for extremely large volumes. This is evident for the results from Gusynin and Reenders.[20] The deviation from the linear behavior is quantitatively important: for the truncation of Gusynin and Reenders a linear extrapolation to the infinite volume results in $N_f^c \approx 2.52$ as compared to the infinite-volume result $N_f^c = 3.2$. (Note that the curve gets extremely steep for the very largest volumes, which are not plotted.) For our results we find a value of $N_f^c \approx 3.23$ for the linear extrapolation, whereas the analytical infinite-volume result is $N_f^c \approx 3.84$. Although this difference is not huge, it highlights the need for nonlinear extrapolation procedures to the infinite-volume limit. Unfortunately our largest volumes are not yet large enough to penetrate this region of nonlinearity.

D. Nonvanishing bare fermion masses

In this subsection we investigate the consequences of explicit bare fermion masses m_0 in the Lagrangian of QED_3 on the chiral phase transition. To this end we determined the properties of the system in the infinite-volume and continuum limit by solving the corresponding DSEs for a range of different bare fermion masses. For any given mass and varying N_f we find that the fermion wave function never develops a pure power law in the infrared. Instead there is a region $0 < p < \Lambda_{IR}$, where the function is constant and a region $\Lambda_{IR} < p < \alpha$ where a power law is present. The scale Λ_{IR} depends on the explicit fermion mass as well as on the number of flavors. We conclude from this that away from the chiral limit the infrared exponent κ is no longer an order parameter. As concerns the global behavior of $Z_f(p^2)$ we still observe the behavior discussed above Eq. (33): at a small

enough momentum p^2 the value of the function $Z_f(p^2)$ increases with N_f up to a certain point at a critical value N_f^c and decreases again if N_f grows further. In the chiral limit this critical value N_f^c marked the chiral phase transition. Here, however, this seems not to be so. The fermion mass function $M(0)$ decreases exponentially with N_f without a trace of a rapid change around N_f^c. We therefore conclude that there is no phase transition in the infinite-volume and continuum limit for QED_3 with nonvanishing bare fermion masses m_0.

On a torus with a given volume, however, the scale $\Lambda_{IR}(N_f)$ decreases with N_f and can become lower than the lowest momentum point p_{min} on the torus. Consequently one then sees a pure power law in $Z_f(p^2)$ for momenta $p_{min} < p < \alpha$. The critical number of fermion flavors N_f^c where this transition is observed coincides with the value of N_f where $Z_f(p_{min}^2)$ is maximal. Thus in a sense one observes a chiral transition on a torus even for nonvanishing m_0 when there is none in the infinite-volume and continuum limit. For the choice $m=0.0024e^2$ the resulting values of N_f^c are plotted against $(Le^2)^{1/3}$ in Fig. 7. Apart from our smallest volumes the resulting values of N_f^c are significantly larger than in the chiral limit. We also observe that in the infinite-volume limit the critical number of flavors goes to infinity, in agreement with our findings discussed in the previous paragraph. Away from the chiral limit QED_3 on a torus shows a chiral phase transition when there is none in the infinite-volume and continuum limit. This implies that extreme care is needed when one attempts to extract information on N_f^c from lattice calculations with finite fermion masses.

Nevertheless it is interesting to compare to lattice results. As explained above the important scale in assessing finite-volume effects is the lowest momentum point available on the torus compared with the generated fermion mass. In our setup with antiperiodic boundary conditions in space and time directions this scale is given by $L_{DSE}=\sqrt{3}\pi/p_{min}$. On the lattice one usually implements antiperiodic boundary conditions in the temporal direction and periodic ones in the two spatial directions. This results in $L_{latt}=\pi/p_{min}$ on the lattice. The couplings are related by $e^2 \simeq 1/(\beta a)$, where β is the dimensionless inverse coupling on the lattice and a the lattice spacing. With $e^2 \simeq 1$ and $\beta \sim \mathcal{O}(1)$ one then obtains $L_{DSE}e^2 \simeq \sqrt{3}L_{latt}\beta$. This means that we should compare the results of contemporary lattice calculations on 80^3-lattices with our values for $L \approx 140$. From the plot of Fig. 7 we then find chiral symmetry breaking for $N_f=1$, whereas at $N_f=1.5$ the system is in the chirally symmetric phase. This is in agreement with recent lattice results[19] and shows that these results are compatible with our value of $N_f^c \approx 3.8$ in the infinite-volume and continuum limit.

Finally we investigate the behavior of the chiral condensate on a torus as a function of the explicit fermion mass. To this end we extract the condensate from our fermion mass function with the help of Eq. (15) at a given fixed ultraviolet momentum cutoff. Our results for $N_f=1.5$ and different box lengths L are shown in Fig. 8. Clearly, for small volumes the condensate decreases linearly with decreasing bare fermion mass m_0 and extrapolates to zero in the chiral limit. For large enough boxes this behavior changes, and we find a finite value in this limit in agreement with results from our continuum DSEs. It is interesting to note that the curves for small volumes are almost degenerate. A volume analysis in this region would therefore indicate weak finite-volume effects where in fact there are large effects when the volume is increased further. Again, this result should serve as a caveat for the interpretation of lattice results.

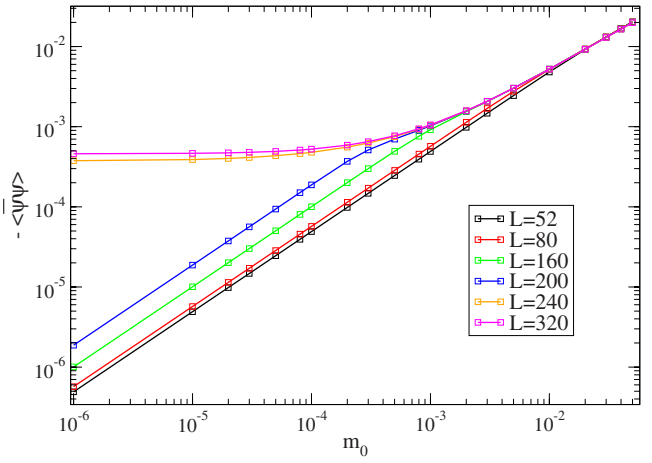

FIG. 8. (Color online) The chiral condensate as a function of the fermion mass for a range of volumes at $N_f=1.5$. Small volumes give rise to a vanishing chiral condensate and are nearly degenerate, falsely indicating weak finite-volume effects.

V. SUMMARY

In this work we investigated volume effects on the chiral phase transition of QED_3 as a function of the number of flavors, N_f. To this end we solved a coupled system of Dyson-Schwinger equations for the fermion and photon dressing functions in the infinite-volume and continuum limit and on a three-torus. We worked in a truncation scheme that in the infinite-volume and continuum limit reproduces a critical number of flavors $N_f^c \approx 3.61-3.84$, a number close to the one obtained with more involved approximation schemes.[5]

Examining the same system on a torus we found considerable volume effects. These can be explained due to the presence of scales of vastly different magnitude in QED_3. On the one hand one has the natural scale $\alpha/e^2=N_f/8$, which is of order one. On the other hand, the dynamically generated fermion masses are orders of magnitude smaller. For example, one has $M(0)=0.05e^2$, for $N_f=1$ as can be seen from Fig. 5. While the first scale remains of the same order, the second one rapidly decreases when the number of flavors becomes larger. When the generated fermion mass drops below the infrared cutoff of the system, given by the inverse of the box length, chiral symmetry breaking disappears and the system falls into the chirally symmetric phase. We quantified these effects and presented results for the critical number of flavors as a function of the box length. They agree qualitatively with corresponding results of Ref. 20 determined in a simpler truncation scheme and a different setup (continuum limit with finite infrared cutoff). Quantitative differences are small.

Our results confirm the notion that lattice calculations at $N_f=1.5$ or $N_f=2$ need very large physical volumes to see dynamical chiral symmetry breaking, let alone quantify their

finite-volume effects. Contemporary lattice results cannot yet accommodate for these and consequently find a system in the chirally symmetric phase in quantitative agreement with our findings. We have shown that these results are nicely compatible with a critical number of flavors $N_f^c \approx 3.61-3.84$ in the infinite-volume and continuum limit.

ACKNOWLEDGMENTS

We are grateful to Lambert Alff and Jan M. Pawlowski for inspiring discussions. This work was supported by a Helmholtz-University Young Investigator Grant No. VH-NG-332.

[1] R. D. Pisarski, Phys. Rev. D **29**, 2423 (1984).
[2] I. F. Herbut, Phys. Rev. B **66**, 094504 (2002); Phys. Rev. Lett. **88**, 047006 (2002).
[3] M. Franz, Z. Tešanović and O. Vafek, Phys. Rev. B **66**, 054535 (2002); Z. Tešanović, O. Vafek, and M. Franz, *ibid.* **65**, 180511(R) (2002); M. Franz and Z. Tešanović, Phys. Rev. Lett. **87**, 257003 (2001).
[4] A. A. Nersesyan and G. E. Vachnadze, J. Low Temp. Phys. **77**, 293 (1989).
[5] C. S. Fischer, R. Alkofer, T. Dahm, and P. Maris, Phys. Rev. D **70**, 073007 (2004).
[6] T. W. Appelquist, M. J. Bowick, D. Karabali, and L. C. R. Wijewardhana, Phys. Rev. D **33**, 3704 (1986).
[7] T. Appelquist, D. Nash, and L. C. R. Wijewardhana, Phys. Rev. Lett. **60**, 2575 (1988).
[8] M. R. Pennington and S. P. Webb, BNL Report No. 40886, 1988 (unpublished).
[9] D. Atkinson, P. W. Johnson, and P. Maris, Phys. Rev. D **42**, 602 (1990).
[10] M. R. Pennington and D. Walsh, Phys. Lett. B **253**, 246 (1991); D. C. Curtis, M. R. Pennington, and D. Walsh, *ibid.* **295**, 313 (1992).
[11] C. J. Burden and C. D. Roberts, Phys. Rev. D **44**, 540 (1991).
[12] P. Maris, Phys. Rev. D **52**, 6087 (1995).
[13] V. P. Gusynin, A. H. Hams, and M. Reenders, Phys. Rev. D **53**, 2227 (1996).
[14] P. Maris, Phys. Rev. D **54**, 4049 (1996).
[15] E. Dagotto, J. B. Kogut, and A. Kocic, Phys. Rev. Lett. **62**, 1083 (1989); Nucl. Phys. B **334**, 279 (1990).
[16] S. Hands and J. B. Kogut, Nucl. Phys. B **335**, 455 (1990).
[17] S. J. Hands, J. B. Kogut, and C. G. Strouthos, Nucl. Phys. B **645**, 321 (2002).
[18] S. J. Hands, J. B. Kogut, L. Scorzato, and C. G. Strouthos, Phys. Rev. B **70**, 104501 (2004).
[19] C. Strouthos and J. B. Kogut, arXiv:0808.2714 (unpublished); C. Strouthos and J. B. Kogut, POS LAT2007 (2007), 278.
[20] V. P. Gusynin and M. Reenders, Phys. Rev. D **68**, 025017 (2003).
[21] C. S. Fischer, R. Alkofer, and H. Reinhardt, Phys. Rev. D **65**, 094008 (2002).
[22] C. S. Fischer, B. Grüter, and R. Alkofer, Ann. Phys. **321**, 1918 (2006).
[23] C. S. Fischer, A. Maas, J. M. Pawlowski, and L. von Smekal, Ann. Phys. **322**, 2916 (2007).
[24] D. C. Curtis and M. R. Pennington, Phys. Rev. D **42**, 4165 (1990).
[25] C. J. Burden and C. D. Roberts, Phys. Rev. D **47**, 5581 (1993).
[26] Z. Dong, H. J. Munczek, and C. D. Roberts, Phys. Lett. B **333**, 536 (1994).
[27] A. Kizilersu, M. Reenders, and M. R. Pennington, Phys. Rev. D **52**, 1242 (1995).
[28] A. Bashir and A. Raya, Phys. Rev. D **64**, 105001 (2001).
[29] A. Bashir, A. Huet, and A. Raya, Phys. Rev. D **66**, 025029 (2002).
[30] A. Bashir and A. Raya, Phys. Rev. D **66**, 105005 (2002).
[31] A. Bashir and A. Raya, Nucl. Phys. B **709**, 307 (2005).
[32] A. Bashir, A. Raya, I. C. Cloet, and C. D. Roberts, Phys. Rev. C **78**, 055201 (2008).
[33] S. Nedelko and J. M. Pawlowski (unpublished).
[34] C. Lerche and L. von Smekal, Phys. Rev. D **65**, 125006 (2002).
[35] D. Zwanziger, Phys. Rev. D **67**, 105001 (2003).
[36] R. Alkofer, C. S. Fischer, and F. J. Llanes-Estrada, Phys. Lett. B **611**, 279 (2005).
[37] C. S. Fischer and J. M. Pawlowski, Phys. Rev. D **75**, 025012 (2007).
[38] C. S. Fischer, A. Maas, and J. M. Pawlowski, arXiv:0810.1987 (unpublished).
[39] H. Leutwyler and A. Smilga, Phys. Rev. D **46**, 5607 (1992).
[40] T. Banks and A. Casher, Nucl. Phys. B **169**, 103 (1980).
[41] C. S. Fischer and M. R. Pennington, Phys. Rev. D **73**, 034029 (2006); Eur. Phys. J. A **31**, 746 (2007).
[42] V. A. Miransky and K. Yamawaki, Phys. Rev. D **55**, 5051 (1997); **56**, 3768 (1997); V. P. Gusynin, V. A. Miransky, and A. V. Shpagin, *ibid.* **58**, 085023 (1998).